ARTICLES

Quasifree inclusive and exclusive analyzing powers at 200 MeV

D. S. Carman,[1,*] L. C. Bland,[1] N. S. Chant,[2] T. Gu,[2] G. M. Huber,[3] J. Huffman,[2] A. Klyachko,[4] B. C. Markham,[1] P. G. Roos,[2] P. Schwandt,[1] and K. Solberg[1]

[1]*Indiana University Cyclotron Facility, Bloomington, Indiana 47408*

[2]*University of Maryland, College Park, Maryland 20742*

[3]*University of Regina, Saskatchewan, Canada S4S 0A2*

[4]*Institute of Nuclear Research, Moscow 117312, Russia*

(Received 16 November 1998)

Analyzing power measurements for both inclusive $(\vec{p},p')$ and exclusive $(\vec{p},2p)$ and $(\vec{p},np)$ quasifree scattering at 200 MeV from ^{2}H and ^{12}C have been completed in the angular range from 27° to 34°. Previous experimental and theoretical work has indicated non-negligible suppression of the inclusive $(\vec{p},p')$ analyzing powers with respect to impulse approximation calculations. Conversely, both suppression and enhancement of the isovector $(\vec{p},n)$ analyzing power data have been found depending on the mass number of the target. Both nonrelativistic and fully relativistic calculations have sought to explain these features. However to address such questions within the inclusive data, it is important to fully understand the makeup of the inclusive spectra. This ensures that any ''nonconventional'' aspects of the data do not arise from contamination of the quasifree scattering yield. [S0556-2813(99)01004-3]

PACS number(s): 25.40.Ep, 21.30.Cb, 24.70.+s, 25.40.Kv

I. INTRODUCTION

The inclusive quasifree scattering (QFS) $(\vec{p},p')$ analyzing power (A_y) has been of experimental interest for a range of nuclei from ^{12}C to ^{208}Pb [1–3] and more recently from light nuclei [4], spanning a range of incident proton energies from 200 to 800 MeV. This interest stems from the strong suppression of the inclusive A_y with respect to free space expectations and impulse approximation (IA) predictions. The theoretical work of Horowitz [5,6] has suggested that this suppression is a direct consequence of the need for IA calculations including fully relativistic dynamics. If true, this would suggest that the data cannot be explained in terms of conventional nuclear physics alone, and that the modification of the free space nucleon-nucleon (NN) interaction by the presence of the spectator nucleons within the nucleus must be taken into account. In this relativistic approach the effective mass of the scattering nucleon within the nuclear environment can be described by a reduced mass m_N^* (where m_N^* is ~80% to 90% of m_N). This reduction of the nucleon mass results as the lower components of the Dirac wave function are enhanced in the nuclear medium due to the presence of strong potentials ($m_N^* = m_N + S$, where S is the average scalar field strength). This m_N^* effect is predicted to significantly enhance the central interaction strength, which results in a dilution or suppression of the A_y. This model also predicts that the inclusive (p,N) cross section and inclusive $(\vec{p},n)$ A_y are relatively insensitive to such effects. However, an alternative explanation for the observed A_y suppression in $(\vec{p},p')$ has been developed within a nonrelativistic model [7–9]. These calculations include the nonlocal couplings in the nuclear response and the fully off-shell behavior of the internucleon force. To this point in time, definitive calculations for different nuclei over a broad range of momentum transfers are not yet available.

While the $(\vec{p},p')$ data in the QF region are strongly suppressed relative to free scattering independent of target or beam energy, the situation for $(\vec{p},n)$ still remains unclear. Published data show both suppression and enhancement of the A_y data depending on the mass number of the target [1]. Thus while the inclusive (p,N) and exclusive (p,Np) cross section data agree reasonably well with IA expectations [10,11], there is a clear disparity with regard to the A_y. Furthermore, whatever is going on has a different effect on the $(\vec{p},p')$ interaction than the $(\vec{p},n)$ interaction. To address such questions within the inclusive data, it is important to fully understand the inclusive spectra. This ensures that any ''nonconventional'' aspects of the data do not arise from some unexpected contamination of the yield.

Inclusive $(\vec{p},p')$ and exclusive $(\vec{p},Np)$ differential cross sections and analyzing powers were measured from CD_2 and ^{12}C targets employing the 200 MeV proton beam at the Indiana University Cyclotron Facility. The ^{2}H results were obtained from a careful subtraction of the two measured yields. Inclusive and exclusive data were acquired concurrently to minimize possible systematic errors in their intercomparison. In order to make n-p and p-p coincidence measurements feasible, a detector with a large figure-of-merit (efficiency ×solid angle=msr) was commissioned for the higher energy ejectile nucleon (n or p) [12]. The 30° central angle of this

*Present address: Department of Physics, Carnegie Mellon University, Pittsburgh, PA 15213.

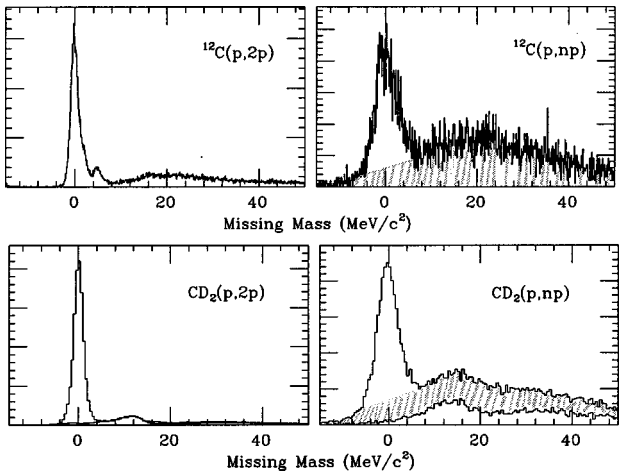

FIG. 1. $^{12}C(p,Np)$ and $CD_2(p,Np)$ missing mass distributions summing over all elements in the ejectile and associated proton detectors. Overlayed on the CD_2 spectra are the normalized ^{12}C contributions. Overlayed on the (p,np) spectra are the background distributions.

detector was chosen to study the nuclear response at a momentum transfer of ~ 1.5 fm^{-1} to be compatible with earlier QFS investigations. The lower energy associated proton was detected in a large solid angle array of NaI which spanned in-plane angles from 34° to 95° and out-of-plane angles from $-5°$ to 28°. This large coverage enabled studies of the exclusive reaction over roughly half of the phase space expected for QFS, which allowed for reliable integration of the exclusive yield to ascertain the extent to which the inclusive (p,p') and (p,n) reactions are dominated by single-step scattering.

Shown in Fig. 1 are our missing mass spectra for the (p,Np) reactions from CD_2 and ^{12}C. These distributions, summed over all elements of the ejectile arm and associated proton arm, highlight the system resolution. The resolution for the (p,np) data is about three times worse than for the $(p,2p)$ data. Overlayed on the CD_2 spectra are the carbon spectra used for subtraction to isolate the deuterium reaction. Overlayed on the (p,np) spectra are the backgrounds from secondary processes occurring in the neutron detector that have been modeled within our detailed Monte Carlo of the system [12].

Our experimental results for the deuterium and carbon cross section data indicate that the factors required to normalize the IA calculations to the data are consistent between the inclusive (p,N) data and the much more restrictive angle-integrated exclusive (p,Np) data [11]. This suggests that the inclusive yield is indeed composed primarily of single-step NN scattering. More complicated reaction dynamics are therefore not expected to significantly contribute to the QFS reaction yield at these energies. Furthermore, the agreement of the predicted quasifree peak position (at the free value shifted by the binding energy), width, and magnitude of the inclusive cross sections for both (p,p') and (p,n), make it clear that there is no strong evidence for the presence of any collective aspects of the nuclear response at these energies. As well, these data clearly demonstrate the appropriateness of the IA framework for the cross section data in this regime.

This present work represents an extension of our cross section results to the analyzing power data. Our goal, given an understanding of the quasifree yield through the cross section data, is then to compare the A_y data to the IA calculations. Comparison of the inclusive to the angle-integrated exclusive results provides further confidence in our understanding of the inclusive yield.

II. QFS CALCULATIONS

In a naive picture of NN QFS, the predicted A_y should agree with the corresponding free space values. This simple picture is modified not only by the bound target nucleon momentum distribution, but to some extent as well by energy-dependent final state interactions. This so-called Maris distortion effect arises due to the energy dependence of the attenuation of the nucleon wavefunction through the target nucleus [13]. In other words, it is produced by the influence of final state interactions forcing p-N collisions to preferentially occur on one side of the nucleus. This results in an effective polarization of the struck nucleons when they are in $l>0$ angular momentum states. The magnitude of the effective polarization depends on the energy difference of the outgoing nucleons in the final state, with the size of the effect becoming larger for larger energy differences. The observed A_y for the $(\vec{p},Np)$ exclusive measurements have contributions from both the A_y of the reaction, as well as the underlying spin correlation coefficient of the p-N interaction. The effective polarization of the knocked-out target nucleon is generated within IA calculations through the absorptive (imaginary) terms of the optical model potential (OMP). On the other hand, the predominantly spin-independent final state interactions are not expected to affect the $(\vec{p},N)$ inclusive A_y which is defined in terms of a ratio of cross sections, thus cancelling these common distortion factors.

The deuterium and carbon $(\vec{p},Np)$ data were analyzed within the IA framework. In this picture, the scattering of a fast incident nucleon by a complex nucleus is approximated by the superposition of the outgoing wave-functions generated by the individual nucleons acting independently, and thus the many-body collision may be decomposed into a superposition of two-body collisions. In this respect, the many-body character of the system represents only a secondary feature. The IA calculations implicitly assume that the incident beam proton never interacts strongly with two target nucleons at the same time, that the amplitude of the incident proton wavefunction is not appreciably diminished in traversing the nucleus, and that the target nucleus binding forces are negligible compared to the forces present during the strong NN interaction [14,15].

The QFS process is represented as a transition from an initial state consisting of an incident proton (a) and a target nucleus (A), to a final state consisting of two outgoing nucleons [the ejectile (c) and the associated nucleon (d)], and a residual nucleus (B). The two scattered nucleons are assumed to have resulted from the QF two-body reaction $b(a,c)d$, where the initial target nucleus is represented as a superposition, $A=B+b$. The momentum of the residual nucleus is assumed unchanged during the scattering process. It acts simply as a spectator and is assumed to carry the missing momentum in the reaction $(\vec{p}_b=-\vec{p}_B)$.

In this work, the deuterium data are compared with plane wave (PWIA) calculations, while the carbon data are compared with distorted wave (DWIA) calculations. The remainder of this section is devoted to a further discussion of the relevant details and limitations regarding these approaches to QFS.

A. Impulse approximation

The PWIA is based upon the assumption that the incident proton interacts with only a single particle within the nucleus, with no other interactions in the entrance or exit channels. In this situation, the wavefunctions for the incident proton and scattered nucleons can be represented by plane waves. For the 200 MeV ^{2}H(p,Np) reaction, the PWIA is a reasonable approximation as the incident proton wavelength ($\sim$2 fm) and the range of the strong NN force ($\sim$1.5 fm) are both less than the average n-p separation in the ^{2}H nucleus ($\sim$2.5 fm). Furthermore, as the deuteron is only very weakly bound ($\sim$2.2 MeV), multiple scattering effects in this QFS channel should be small.

For the ^{2}H calculations, the standard Hulthen form for the deuteron wavefunction was employed [16,17]. In this parametrization of the coordinate space wave function, only the s-wave contribution is modeled, while the d-wave contribution is ignored. The calculated ^{2}H$(\vec{p},Np)$ A_y is given by the free NN value evaluated at the appropriate beam energy and scattering angles for the three-body final state.

For nuclei much heavier than ^{2}H, the internucleon spacing and the wavelength of the incident proton are comparable, and thus multiple scattering effects become more important and can no longer be ignored. This multiple scattering causes the incident and outgoing nucleon plane waves to become distorted. As well, the strong absorption of the incoming and outgoing nucleon flux by the nucleus must be taken into account. It is in this realm that the DWIA calculations become necessary to reliably predict the variation of the A_y with scattering angle and energy. Furthermore, comparisons of data to these calculations may enable us to observe deviations from the IA, i.e., effects on the scattering nucleons due to their presence within the nuclear medium.

The ^{12}C data are compared with THREEDEE DWIA calculations [18] which represents a quantum mechanical treatment of the scattering process that relies on the factorization approximation. The strong final state interactions are incorporated by using scattering state wave functions which are solutions to the Schrödinger equation including a complex spin and energy-dependent OMP.

The Nadasen-Schwandt potential was employed for our DWIA calculations [19,20]. This potential was deduced from fits to an extensive set of cross section and A_y measurements for proton elastic scattering from ^{40}Ca, ^{90}Zr, and ^{208}Pb over the proton energy range from 60 to 180 MeV, detecting the elastically scattered protons over the angular range from 6° to 90°. These fits served to generate a broad range phenomenological OMP for nucleon-nucleus scattering. This OMP was selected due to the compatibility of the energy and angular range of the fits with respect to the kinematics of our data set.

Although the cross section and A_y data employed in the fits went down to an energy of 60 MeV, extrapolations of the potential to energies below even 40 MeV matched reasonably well with results of previous lower energy analyses. The fact that the associated protons in our $(\vec{p},Np)$ measurements were included in the analysis down to $\sim$10 MeV implies that the OMP was further extrapolated by nearly another 30 MeV. This is a weakness in the calculation that could be rectified by merging the Nadasen-Schwandt OMP with a potential that fits lower energy nucleon-nucleus elastic scattering (e.g., the Becchetti OMP fits $A \geqslant 40$, $10 \leqslant T_p \leqslant 50$ MeV [21]).

In the QF (p,Np) knockout reaction, the invariant mass of the struck nucleon is shifted from its free space value m_N by $-(E_B + p_R^2/2\mu)$, where E_B is the binding energy of the struck nucleon, p_R is the recoil momentum of the $(A-1)$ residual, and μ is the reduced mass of the nucleon/$(A-1)$ system. In this picture, the struck nucleon is always off-shell by at least E_B. As this is deemed not too far off-shell, an additional simplification in the two-body scattering amplitude is employed by evaluating it fully on-shell. This assumption though allows for some ambiguities in the evaluation of the amplitude regarding the appropriate assignment of the energy in the two-body scattering system. Two such assumptions are called the initial and final energy prescriptions (IEP,FEP). In the FEP, the two-body amplitude is evaluated at the total energy as determined within the center-of-mass (c.m.) of the two outgoing nucleons, where both are fully on-shell. In the IEP, the two-body amplitude is evaluated at the total energy as determined within the c.m. of the incident proton and the struck target nucleon. These energies differ roughly by the binding energies involved: $\sim$2.2 MeV for ^{2}H(p,Np) and $\sim$16 MeV for ^{12}C(p,Np). The NN cross sections and scattering amplitudes employed are calculated using the results from the Arndt database [22].

B. Exclusive calculations

The exclusive A_y for each reaction has been calculated on a grid of the variables T_c (the kinetic energy of the ejectile), along with Θ_d and β_d (the in-plane and out-of-plane angles for the associated nucleon). Variation of any of these kinematic quantities results in a change in the target nucleon momentum, which in the present model, is assumed equal to the spectator $(A-1)$ core momentum. The angles Θ_d and β_d represent the natural independent variables to employ for the exclusive analysis since it is necessary to integrate over them to determine that portion of the inclusive yield attributable to valence shell knockout. In this sense, study of the exclusive data with respect to Θ_d provides a direct representation of the inclusive ''integrand.'' For the exclusive data analysis, a single bin of β_d is employed, and the Θ_d dependence of the exclusive observables is studied for different values of T_c crossing over the expected peak of the QFS response.

All data were acquired with the central angle of the ejectile arm at $\Theta_c = 30.4°$. The Θ_c binning employed corresponds either to the full acceptance of the ejectile nucleon detector, or to the ejectile arm acceptance divided into three equal bins (corresponding roughly to 27°, 30°, and 34°). In each case, the QFS response peak is expected to occur at roughly

$$T_c = T_a \cos^2 \Theta_c - E_B . \quad (1)$$

C. Angle-integrated exclusive and inclusive calculations

The angle-integrated A_y was determined by first calculating the exclusive A_y on a grid of Θ_d/β_d roughly matched to the associated proton detector acceptance for each choice of T_c and Θ_c. This angular grid must be chosen finely enough to account for the rapid variations of the observables, generally caused by the angular dependence of the momentum space wave-function of the struck nucleon. It is possible that some deficiencies of the angle-integrated calculations with respect to the data may be attributable to employment of an inadequate grid size, a statement which applies as well to the inclusive observable calculations. Over the angular ranges $30° \leqslant \Theta_d \leqslant 96°$, $0° \leqslant \beta_d \leqslant 28°$, a grid size was selected with $N_\Theta = 67$, $N_\beta = 15$, where $N_{\Theta,\beta}$ represent the number of grid points within each angular range.

The angle-integrated observables were then calculated from this exclusive observable grid by performing an integration over the known associated nucleon acceptance in Θ_d/β_d. The spin-dependent partial cross sections required to compute the A_y are given by

$$\frac{d^2\sigma}{d\Omega_c dE_c} A_y(T_c,\Theta_c) = \int d\beta_d \cos\beta_d \int d\Theta_d \times \frac{d^3\sigma}{d\Omega_c d\Omega_d dE_c} A_y^E(T_c,\Theta_c,\Theta_d,\beta_d). \tag{2}$$

Here A_y^E represents the exclusive A_y determined at each Θ_d/β_d grid point (averaged over the bin acceptance). These angle-integrated quantities were determined as a function of ω_c, the energy transfer to the ejectile nucleon, to be compatible with the presentation of the inclusive results.

To compare the integrated exclusive calculations with the data, the individual calculations for each shell model orbital were added together incoherently, weighting the calculations for each orbital by spectroscopic factors (SF) determined directly from the cross section data. Thus for combined knockout from the $3/2^-$ and $1/2^-$ states from ^{12}C, the calculated A_y is given by

$$A_y = \frac{(\sigma\cdot SF\cdot A_y)^{3/2^-} + (\sigma\cdot SF\cdot A_y)^{1/2^-}}{(\sigma\cdot SF)^{3/2^-} + (\sigma\cdot SF)^{1/2^-}}. \tag{3}$$

The inclusive calculations were performed in a spirit similar to the angle-integrated exclusive calculations. In principle, the integrations should be completed over the full solid angle for the unobserved particle ($0 \leqslant \Theta_d \leqslant 2\pi$, $-\pi \leqslant \beta_d \leqslant \pi$). In practice though, this is not done because it is impractical from the standpoint of required calculation times, the required large extrapolations of the OMP to extremely low energies for the scattering states of interest, as well as the assumptions regarding the distribution of the inclusive QFS yields. For the inclusive calculations it is generally assumed that the associated proton distribution is confined to a cone around the zero recoil momentum point given by

$$\Theta_d^{ZR} = \cos^{-1}\left(\frac{p_a - p_c\cos\Theta_c}{p_d}\right). \tag{4}$$

The overall width of the associated nucleon cone about Θ_d^{ZR} is governed by the expectation value of the radial coordinate of the struck nucleon relative to the c.m. of the target nucleus. The radial dependence of the eigenfunctions goes as r^l as $r \to 0$, thus as the orbital angular momentum l increases, the probability that the nucleon is at small r is extremely small. As the expectation value of the radial probability distribution increases, the half-angle of the knockout nucleon cone will correspondingly increase. The cone for ^{12}C, dominated by p-shell knockout, will clearly be larger than for ^{2}H, which is dominated by s-shell knockout.

In the inclusive THREEDEE calculations, the imaginary parts of the OMP for the associated nucleon are set to zero as there is no loss of flux in the inclusive yield if the associated particle is not observed. The associated nucleon scattering states are calculated in a purely real potential following the procedure of Wesick [23]. Note that in this model description, as opposed to other models of the continuum such as the slab model [24], the conditions of the Pauli exclusion principle are naturally included since the kinematics and phase space factors require the unobserved associated nucleon to make a transition into the continuum if the residual $(A-1)$ system is assumed to be in a bound state. Finally, separate calculations were performed for both proton $(\vec{p},2p)$ and neutron $(\vec{p},pn)$ knockout for the associated nucleon for the inclusive ^{2}H$(\vec{p},p')$ and ^{12}C$(\vec{p},p')$ reactions, and the results were added together incoherently. The inclusive calculations employed the integration limits $5° \leqslant \Theta_d \leqslant 180°$, $0° \leqslant \beta_d \leqslant 90°$, with $N_\Theta = 25$, $N_\beta = 14$.

III. ANALYZING POWER RESULTS

The A_y results were extracted from the corrected yields for each reaction gated separately by incident protons with spin up and spin down relative to the horizontal reaction plane defined by the beam and ejectile nucleon momentum vectors. The corrected yields are given by

$$Y_{\rm corr}^{u,d} = (Y_p^{u,d} - R_L^{u,d}\cdot Y_c^{u,d} - Y_{\rm acc}^{u,d}) F_{\rm corr}^{u,d}. \tag{5}$$

In this expression, the $Y_i^{u,d}$ terms represent the spin gated yields of interest for the inclusive, angle-integrated exclusive, and exclusive data. Y_p represents the primary reaction yield, either CD_2 or ^{12}C. Y_c represents the background contribution from the ^{12}C content of the CD_2 target. The factor R_L, which represents the overall normalization of the ^{12}C data set relative to the CD_2 data set, is given by the ratio of the live time corrected integrated luminosities of the two data samples. These factors differed slightly between the inclusive singles data ($R_L = 0.874$) and the exclusive data ($R_L = 1.0531$) due to the differences in live times between the event streams. These R_L factors close to unity indicate that the CD_2 spectra and the ^{12}C spectra were well matched for comparison. $Y_{\rm acc}$ represents the average contribution of accidental coincidences within the real time coincidence peak. The average of the accidental yields from beam bursts just before and just after the real time peak was subtracted from each bin. Due to the extremely favorable reals to accidental ratio for all of the $(p,2p)$ data, this accidental yield was nonzero only for the coincidence (p,np) data sets. Finally, the factor $F_{\rm corr}^{u,d}$ represents a correction to the spin gated yields

due to the slight differences in the spin up and spin down computer live times, as well as the slight difference between the number of incident protons with spin up and spin down.

With these yields extracted for each desired energy and angle bin, the A_y is then given by

$$A_y = \frac{Y^u_{\rm corr} - Y^d_{\rm corr}}{P(Y^u_{\rm corr} + Y^d_{\rm corr})}. \tag{6}$$

Here P represents the average of the spin up and spin down polarizations of the beam. This definition of the A_y is given in accordance with the so-called Madison convention. For the deuterium and carbon $(\vec{p},Np)$ data the beam polarization was determined to be $P = 0.70 \pm 0.02$. The statistical uncertainty in this quantity is given by

$$\delta A_y = \sqrt{\frac{1 - P^2 \cdot A_y^2}{P^2(Y^u_{\rm corr} + Y^d_{\rm corr})}}. \tag{7}$$

Although this expression is not strictly valid if $P_u \neq P_d$, it is satisfactory to first order. It is this quantity representing the statistical uncertainty that is displayed as the error bars on all of the data shown in this work. However, the beam polarization magnitude differences can be taken into account exactly

$$A_y = \frac{A'_y}{1 - \delta A'_y}. \tag{8}$$

In this expression, A'_y is obtained with $P = \frac{1}{2}(P^u + P^d)$, and δ represents the difference quantity $\frac{1}{2}(P^u - P^d)$. As determined from polarimeter measurements during the $(\vec{p},2p)$ and $(\vec{p},np)$ running sequences, the value of δ was given in both instances by 0.012. Therefore these corrections to the A_y are on the order of 0.5%.

Another systematic uncertainty in the measurements arises from the uncertainty in the measured polarization of the incident beam. Typical uncertainties in the value of P were about 1.5%. This uncertainty in the average beam polarization contributes to the uncertainty in the A_y a term given by

$$\delta A_y = A_y \frac{\Delta P}{P}. \tag{9}$$

This uncertainty is also negligible relative to the typical statistical uncertainties in the measurements of $\delta A_y = 0.05$ for the $(\vec{p},2p)$ data, and $\delta A_y = 0.35$ for the $(\vec{p},np)$ data.

A. Exclusive data

The exclusive data are shown as a function of Θ_d gated by a particular angular range for the ejectile nucleon. To facilitate comparisons between the $(\vec{p},2p)$ and $(\vec{p},np)$ data sets, care has been taken to sort the data in a consistent manner to match the relevant energy and angle binning parameters.

Detailed study of the exclusive data over a broad range of final state kinematics provides another distinct avenue, beyond the cross section data, to probe the QFS reaction dynamics. For the PWIA $d(\vec{p},Np)$ calculations, the NN interaction alone is responsible for the A_y, and thus it should provide a very good representation of the data due to the expectation that multiple scattering effects in deuterium are minimal. For the DWIA ^{12}C$(\vec{p},Np)$ calculations however, the A_y depends on both the distorting optical potential and the spin dependence of the NN interaction. Therefore the predictions for ^{12}C can provide a rather strong benchmark for testing the applicability of the Nadasen-Schwandt OMP employed for this work.

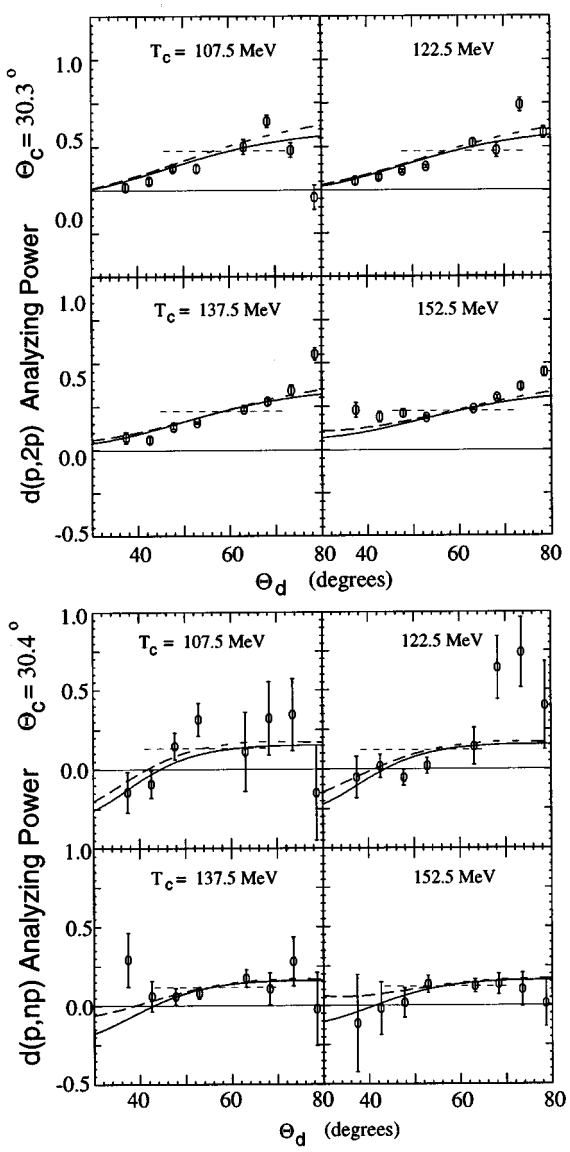

FIG. 2. $d(\vec{p},Np)$ exclusive A_y as a function of Θ_d summed over the full acceptance of the ejectile arm detector.

The ^{2}H$(\vec{p},Np)$ exclusive A_y data are presented in Fig. 2 compared with THREEDEE PWIA calculations. The data were sorted as a function of Θ_d for four different ejectile energy bins ($T_c = 107.5$, 122.5, 137.5, 152.5 MeV) and were summed over the full acceptance of the ejectile arm specifically to reduce the statistical uncertainty with the (p,np) data set. In Fig. 2 and in all subsequent figures, the solid curves represent the calculations assuming the on-shell FEP approximation and the dashed curves represent the IEP approximation. The sort dashed segments mark the free NN A_y prediction [22].

The PWIA predictions are seen to agree very satisfactorily with the data, particularly for $d(\vec{p},2p)$. While the agreement remains good for $d(\vec{p},np)$, it is clear that away from the peak of the response about the zero recoil momentum point ($\Theta_d \sim 55°$), the data are dominated by the statistical uncertainties. It is also seen that the comparisons made with the data are not particularly sensitive to the choice of the on-shell approximations for the kinematics.

The $^{12}C(\vec{p},Np)$ exclusive A_y data are compared with the predictions of the THREEDEE DWIA calculations. The first phase of the analysis was to study the data for the $^{12}C(\vec{p},2p)$ reaction separately for p-shell knockout from the $3/2^-$ ground state and $1/2^-$ first excited state. This analysis was performed using a Gaussian fitting procedure on the spin up and spin down gated yields. This process was necessary as the ~2.0 MeV missing mass resolution of the coincidence detection system was insufficient to fully separate these states. The fits for the spin up and spin down yields were performed separately, and the centroids and widths of the fitted Gaussian peaks were allowed to be completely independent. This procedure was carried out as it resulted in the best overall χ^2 values for the fits over all data bins. This procedure though gives rise to a small systematic error within the analysis of the $1p_{3/2}$ and $1p_{1/2}$ data. However, the summed p-shell knockout data are unaffected by this procedure as the analysis was performed by integrating the missing mass spectra over the appropriate region.

The $^{12}C(\vec{p},2p)$ data, gated separately on the $1p$ hole states, are presented in Fig. 3 for three ejectile angle bins ($\Theta_c = 27°, 30°, 34°$) and three ejectile energy bins ($T_c = 105, 125, 145$ MeV). The DWIA calculations provide a satisfactory representation of the data, particularly for the $3/2^-$ ground state. The trends of the $1/2^-$ data are reasonably reproduced, however, these data are statistically limited, and also systematically limited by the Gaussian fitting technique. Overall, the quality of the fits, as seen through the average value of the χ^2 per degree of freedom, was found to be quite reasonable. Note that the error bars in Fig. 3 represent only the associated statistical uncertainties.

These exclusive data provide strong confirmation of the applicability of the Nadasen-Schwandt OMP for the carbon data. The exclusive A_y is affected by energy-dependent distortions on the low energy associated nucleon flux resulting in an effective polarization of the target nucleon. This effective polarization is modeled within the DWIA calculation through the absorption caused by the imaginary terms of the potential. Therefore the level of detailed agreement seen in this observable gives confidence in the quality of this input to the DWIA over the energy range of this potential.

The model clearly predicts the appropriate sign of the polarization for both the $3/2^-$ and $1/2^-$ states, and furthermore, as seen through the $3/2^-$ knockout especially, the modeling of the absorptive aspects of the potential over a very broad range of final state kinematics (and hence over a very broad range of the momentum space wave function of the target nucleon) is quite appropriate. As well, the model correctly predicts the opposite sign for the struck nucleon polarization at angles about the zero recoil momentum point. Note also that the effective polarization increases as the ejectile energy increases. This results as the distortion effects on the low energy associated proton increase as T_c increases

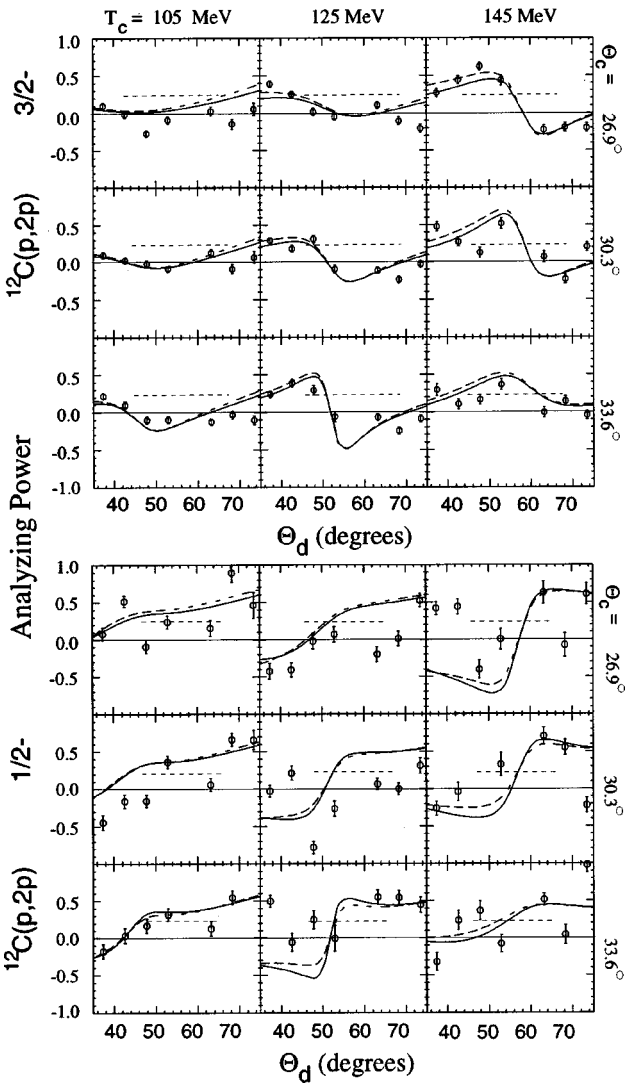

FIG. 3. $^{12}C(\vec{p},2p)$ exclusive A_y separated as a function of Θ_d for $1p$ shell knockout from the $3/2^-$ ground state and $1/2^-$ first excited state.

(and hence as T_d decreases). This is clearly seen within the data and further serves to demonstrate that the effective polarization in this Maris effect arises through the distortions.

The $^{12}C(\vec{p},Np)$ exclusive data are presented for comparison in Fig. 4 summed over the two p-shell hole states. It remains the case that the DWIA calculations satisfactorily follow the data for both proton and neutron knockout. The calculations for the individual shell model orbitals were added together incoherently as shown in Eq. (3). The occupation numbers employed were extracted from the DWIA fit to the exclusive cross section data, $N_{3/2^-} = 4.0$, $N_{1/2^-} = 1.0$. Again, the data do not show preference for the choice of the on-shell approximation to the kinematics, as both appear to provide an equally valid description of the data given the statistical uncertainties. Note that for the highest two ejectile energy bins (and hence the lowest associated nucleon energies) that there remains some evidence of the effective polarization. This remnant effect would not be present for a filled p-shell target such as ^{16}O where the equal and opposite polarizations for the $3/2^-$ and $1/2^-$ knockout would cancel out when summing over the two states.

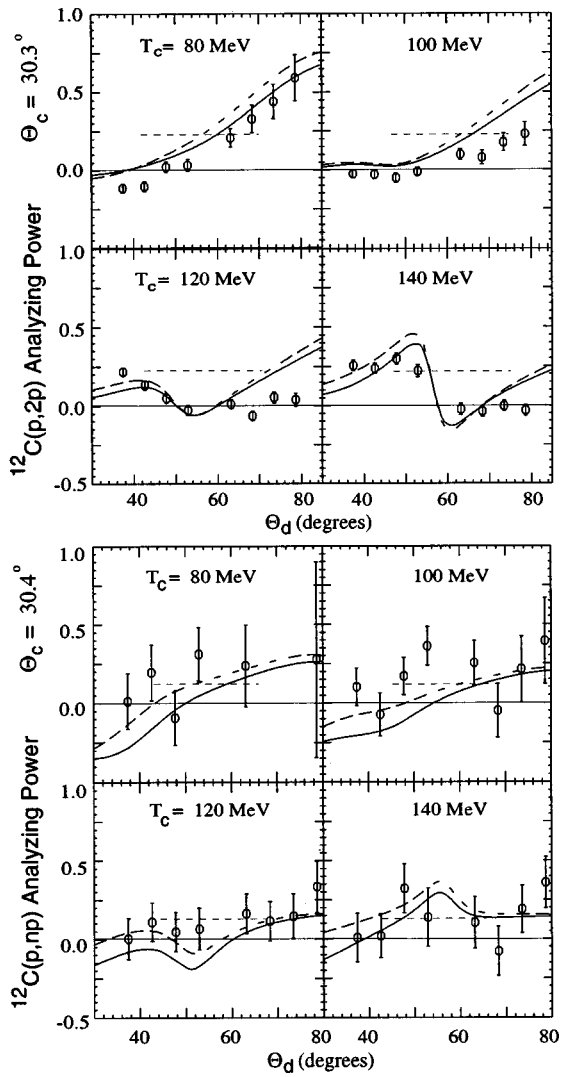

FIG. 4. $^{12}C(\vec{p},Np)$ exclusive A_y for $1p$ shell knockout as a function of Θ_d summed over the full acceptance of the ejectile detector. The spectroscopic factors used in the calculations were given by $N_{3/2^-}=4.0$ and $N_{1/2^-}=1.0$.

B. Integrated exclusive data

The angle-integrated exclusive A_y for deuterium and carbon are shown in this section as a function of ω_c gated by a particular angular range for the ejectile nucleon. Again, care has been taken to sort the $(\vec{p},2p)$ and $(\vec{p},np)$ data in a consistent manner. Beyond our detailed comparisons of the inclusive and exclusive cross section data [10,11], agreement between the angle-integrated and the inclusive A_y data sets, due to the very strict event selection with the exclusive measurement, can then give us confidence that the inclusive yields are composed primarily of single-step NN scattering. Due to the large angular coverage of our detector array for the associated nucleon, our angle-integrated exclusive data should provide a portent of what can be expected from the inclusive data.

The $^2H(\vec{p},Np)$ angle-integrated exclusive A_y data are presented in Fig. 5 for three ejectile angle bins (Θ_c $=27°,30°,34°$). In this plot and in all subsequent plots the vertical arrow represents the expected location of the QFS peak from $\omega_{NN}+Q$, where Q is the Q value of the reaction.

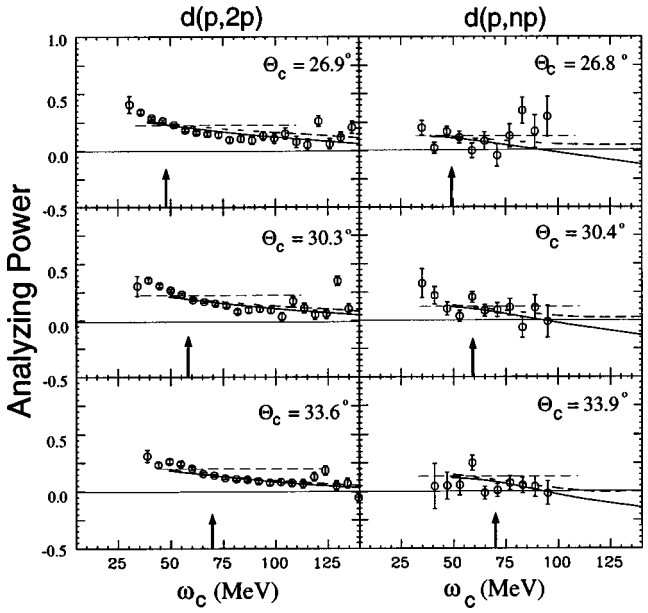

FIG. 5. $d(\vec{p},Np)$ angle-integrated A_y plotted as a function of the energy transfer ω_c.

The agreement between the $d(\vec{p},2p)$ data and the plane wave calculation is quite satisfactory, agreeing within the statistical errors. A number of features are also apparent within each angle bin. First, at values of $\omega_c<55$ MeV, the data appears to begin to move above the PWIA prediction. This effect appears consistent with a small p-d elastic scattering contaminant which enters into the final spectra through the looseness of the particle identification cuts. Second, the data dips below the plane wave result above ω_c ≈ 70 MeV. This effect is most apparent in the two smaller angle bins. This is in good agreement with the data of Li [25]. This effect could be described as a suppression of the data relative to the calculation to put this interpretation on the same footing as the $^{12}C(\vec{p},2p)$ analysis shown in the next section, however without more evidence, this description is not necessarily with foundation.

The $d(\vec{p},np)$ data does not lend itself to an in-depth comparison to the plane wave calculation due to the statistical limitations of the data. The only point that can be made is that the data and the calculation agree to within the error bars.

The $^{12}C(\vec{p},Np)$ angle-integrated exclusive A_y data are presented in Fig. 6 for three ejectile angle bins (Θ_c $=27°,30°,34°$). The data were summed over both the $3/2^-$ ground and $1/2^-$ first excited states.

The first thing noticed in studying the $^{12}C(\vec{p},2p)$ results is the clear suppression of the data for all kinematics relative to the DWIA predictions. This broad range disagreement of the calculations with the data is the first unambiguous breakdown of the IA formalism in the present study. It indicates that the conventional theoretical model employed is missing some relevant aspect of the physics. Given that the integrated exclusive yields extracted to determine these A_y data are gated by missing mass with appropriate background subtractions (see Fig. 1), it is not likely that these data are affected by any significant level of background contamination which might be responsible for the effect. On the other hand, the same suppression is not present within the $^{12}C(\vec{p},np)$ data. It

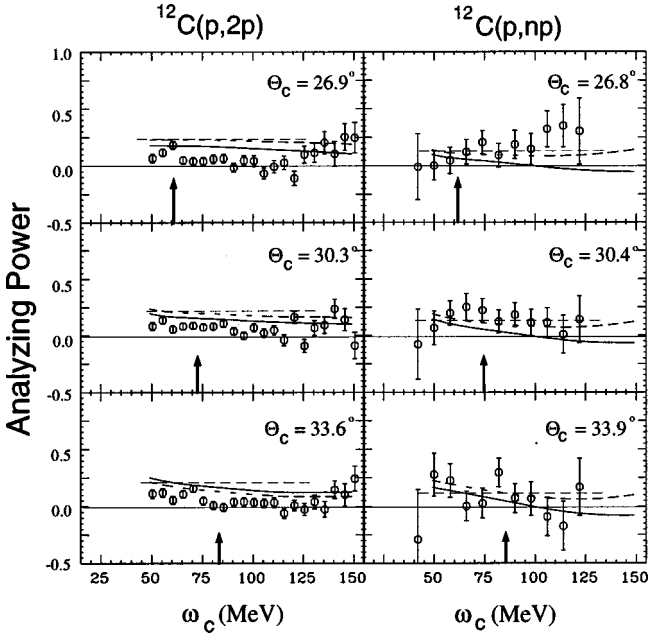

FIG. 6. ^{12}C($\vec{p}$,Np) angle-integrated A_y for $1p$ shell knockout plotted as a function of the energy transfer to the ejectile nucleon ω_c. The spectroscopic factors used in the calculations were $N_{3/2^-}=3.7$ and $N_{1/2^-}=0.85$.

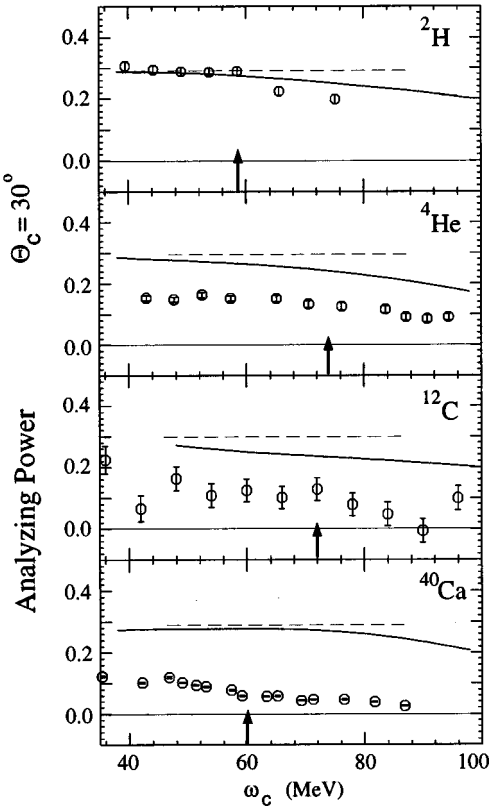

FIG. 7. Inclusive ($\vec{p}$,p') A_y as a function of the energy transfer ω_c. The deuterium and carbon data are from this work, while the helium data is from [25] and the calcium data is from [2]. All IA calculations shown employ the FEP on-shell approximation.

appears instead that the data are slightly enhanced relative to the DWIA predictions, and in fact, agree reasonably well with free scattering predictions. This statement is only a qualitative observation due to the level of statistical accuracy of the data set.

C. Inclusive data

The inclusive data are presented in Fig. 7 for ^{2}H, ^{4}He, ^{12}C, and ^{40}Ca at $\Theta_c=30°$. The ^{4}He($\vec{p}$,p') and ^{40}Ca($\vec{p}$,p') data, from [25] and [2] respectively, have been included to present a more comprehensive picture of the failure of the IA to explain certain features of the data. Again, the vertical arrows mark the expected location of the QFS response peak from $\omega_{NN}+Q$. Note that since the associated nucleon can be either a proton or a neutron, the free NN A_y represents the isospin average of the free p-p and p-n A_y. The IA calculations represent the incoherent average of the ($\vec{p}$,$2p$) and ($\vec{p}$,np) calculations, with equal weighting factors assigned to the cross sections.

The inclusive ($\vec{p}$,p') data appear suppressed relative to the IA calculations. The magnitude of the suppression seen for the d($\vec{p}$,p') and ^{12}C($\vec{p}$,p') data is consistent with what was seen within the angle-integrated exclusive data. Qualitatively, the suppression observed follows the trend of the nuclear density in that it appears to increase monotonically in going from ^{2}H to ^{40}Ca. The suppression of the data seen here with respect to the IA calculations is of the same order of magnitude as that seen at higher energy [1]. It is this suppression that cannot be explained by the conventional theoretical model that provides strong evidence for a so-called medium modification effect. If the interpretation included above regarding the trend of the suppression with increasing mass number of the target is sensible, this would suggest that the deviations are largest where the nuclear density is the largest. This is certainly how one might expect these medium modifications to manifest themselves. Note that the suppression has been attributed to a sensitive cancellation between the large scalar and vector potentials that apply in relativistic models for this process. In this same framework the ($\vec{p}$,n) QFS A_y is predicted to be very close to free scattering expectations [5,6], in reasonable agreement with what has been seen through the d($\vec{p}$,np) and ^{12}C($\vec{p}$,np) integrated exclusive data.

IV. SUMMARY AND CONCLUSIONS

Analyzing power data have been presented compared with either PWIA or DWIA calculations. Our main goal in this analysis was to test the validity of the IA in an energy regime where the QFS reaction dynamics can be attributed to single-step scattering. Previous experimental and theoretical work has indicated non-negligible deviations of the inclusive ($\vec{p}$,p') QFS A_y from expectations of the IA description. Conversely, these deviations have not been seen with the isovector ($\vec{p}$,n) A_y. Our data have yielded results consistent with these earlier inclusive QFS studies. The suppression of the ($\vec{p}$,p') A_y is observed for both the inclusive data and the much more selective angle-integrated exclusive data. This indicates that the effect cannot be attributed to a contamination of the inclusive yield from either non-QF background or from more complicated reaction dynamics such as multi-

nucleon knockout or cluster knockout processes. This provides very strong evidence that this effect results from a modification of the NN scattering process within the nuclear environment. By studying the $(\vec{p},p')$ data as a function of target mass number, the medium modification effect observed appears to increase as a function of the nuclear density. Also worthy of mention is that the A_y is apparently uniquely sensitive to this medium modification effect at these energies.

ACKNOWLEDGMENTS

This work was carried out under NSF Contract No. NSF-PHY-93-14783 NUC RES and the Natural Sciences and Engineering Research Council of Canada (NSERC).

[1] K. Hicks *et al.*, in *Intersections Between Nuclear and Particle Physics*, edited by G. M. Bunce, AIP Conf. Proc. No. 176 (AIP, New York, 1988), p. 26.
[2] L. C. Bland, in Correlations in Hadronic Systems, Proceedings of the 8th Mini-Conference ''Correlations in Hadronic Systems,'' edited by E. Jans, L. Lapikas, P. J. Mulders, and J. Oberski (NIKHEF, Amsterdam, 1994), p. 64.
[3] P. Kitching *et al.*, Nucl. Phys. **A340**, 423 (1980).
[4] K. Hicks *et al.*, Phys. Rev. C **47**, 260 (1993).
[5] C. Horowitz and M. Iqbal, Phys. Rev. C **33**, 2059 (1986).
[6] C. Horowitz and D. Murdock, Phys. Rev. C **37**, 2032 (1988).
[7] F. A. Brieva and W. G. Love, Phys. Rev. C **42**, 2573 (1990).
[8] H. F. Arellano *et al.*, Phys. Rev. C **43**, 1875 (1991).
[9] H. F. Arellano *et al.*, Phys. Rev. C **54**, 2570 (1996).
[10] D. S. Carman *et al.*, in *Eighth International Symposium on Polarization Phenomena in Nuclear Physics*, edited by E. J. Stephenson and S. E. Vigdor, AIP Conf. Proc. No. 339 (AIP, New York, 1995), p. 444.
[11] D. S. Carman *et al.*, Phys. Lett. B (to be published).
[12] D. S. Carman *et al.*, Nucl. Instrum. Methods Phys. Res. A (to be published).
[13] G. Jacob *et al.*, Nucl. Phys. **A257**, 517 (1976).
[14] Chew, Phys. Rev. **80**, 196 (1950).
[15] Chew and Wick, Phys. Rev. **85**, 636 (1952).
[16] A. F. Kuckes *et al.*, Ann. Phys. (N.Y.) **15**, 193 (1961).
[17] T. K. Lim, Nucl. Phys. **A129**, 259 (1969).
[18] N. S. Chant and P. G. Roos, Phys. Rev. C **15**, 57 (1977).
[19] A. Nadasen *et al.*, Phys. Rev. C **23**, 1023 (1981).
[20] P. Schwandt *et al.*, Phys. Rev. C **26**, 55 (1982).
[21] F. D. Becchetti and G. W. Greenlees, Phys. Rev. **182**, 1190 (1969).
[22] Arndt and Roper, SAID Program, phase shift solution SM89.
[23] J. S. Wesick *et al.*, Phys. Rev. C **32**, 1474 (1985).
[24] G. F. Bertsch and O. Scholten, Phys. Rev. C **25**, 804 (1982).
[25] P. Li, Ph.D. thesis, Indiana University, 1994.